Electronic Supplementary Material (ESI) for Journal of Materials Chemistry A.


# Grain boundary strain localization in a CdTe solar cell revealed by Scanning 3D X-ray diffraction microscopy

A. Shukla [a], J. Wright [e], A. Henningsson [d], H. Stieglitz [b], E. Colegrove [f], L. Besley [a], C. Baur [a], S.D. Angelis [a], M. Stuckelberger [c], H.F. Poulsen [a], J.W. Andreasen* [a]

[a] Technical University of Denmark, Fysikvej Building 310, Lyngby, Denmark, [b] European Synchrotron Radiation Facility, 71 Av. des Martyrs, Grenoble, France, [c] Lund University, Ole Römers väg 1, Lund, Sweden, [d] Helmholtz-Zentrum Geesthacht, Max-Planck-Straße 1, 21502, Geesthacht, Germany, [e] National Renewable Energy Laboratory, Golden, CO 80401, United States of America, [f] Deutsches Elektronen-Synchrotron DESY, Notkestraße 85, Hamburg, Germany.

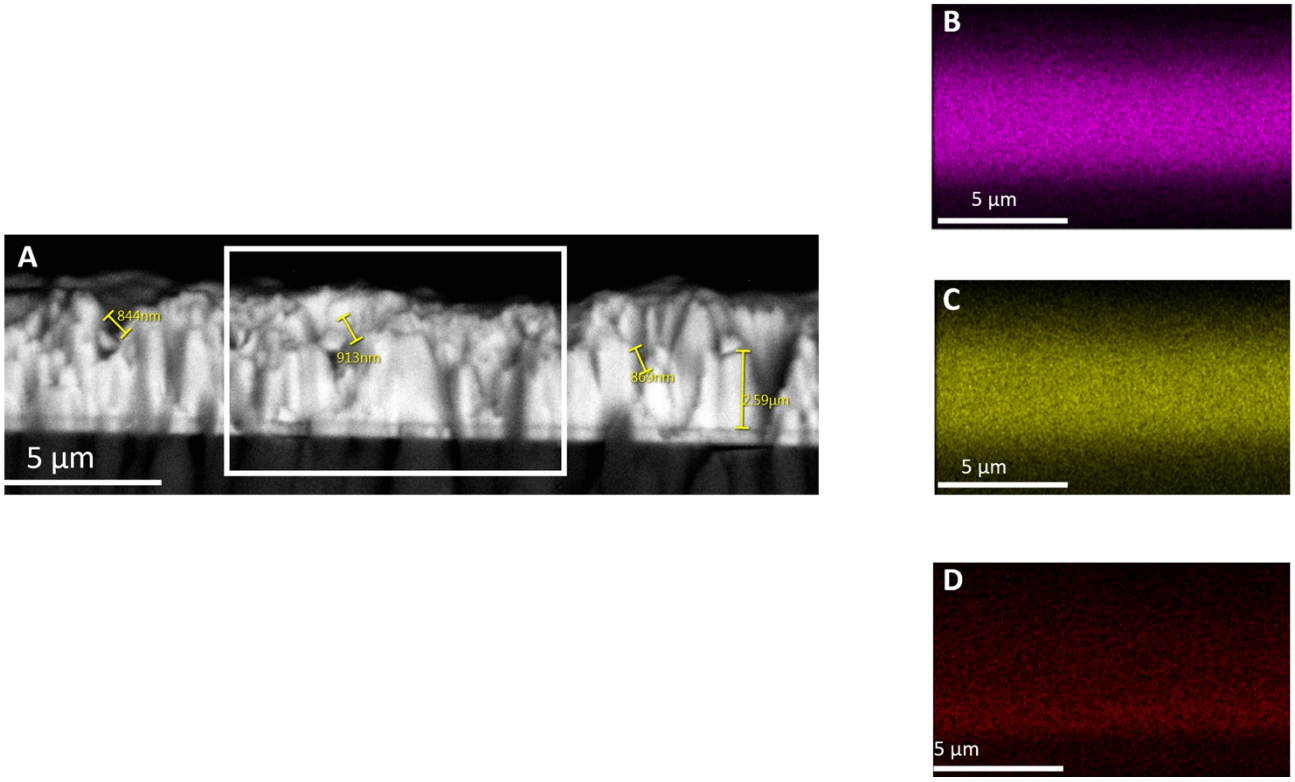


Figure S1. A) SEM image of CdTe thin film cross-section showing columnar grains. B) EDS mapping of region highlighted in A). B) Cadmium EDS map C) Tellurium EDS map D) Sulfur EDS map. The dense red line in D is the CdS electrode. It is clear that some amount of sulfur diffuses in the CdTe layer.

From Figure S1.B and Figure S1.C, it can be inferred that Te diffuses more into the substrate than Cd (Tellurium EDS map has more fringes around it than the Cadmium EDS map). This is an indication of interdiffusion of Tellurium and Sulfur.

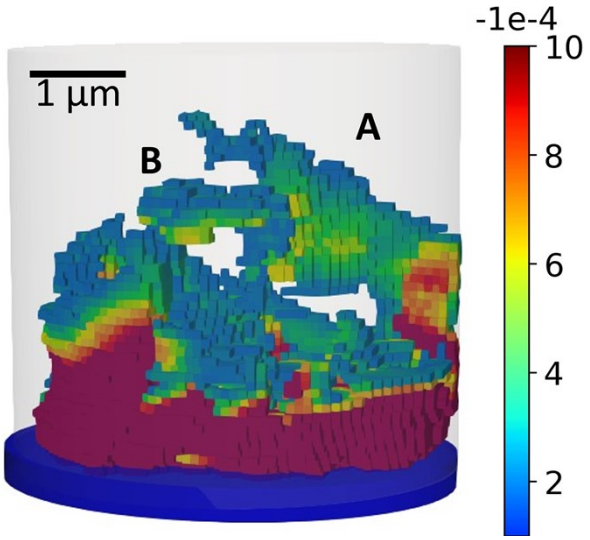


Figure S2. 3D representation of high-strain areas in the CdTe absorber layer. The transparent cylinder in the reconstruction illustrates the sample volume. The purple disk at the bottom is the schematic for the n-type CdS layer. Points A and B are regions shown in Figure 4 and Figure 5, respectively.

| Grain Boundary (s) | Average misorientation (deg) | Is a twin boundary? | Strain localization |
|---|---|---|---|
| a | 13 | No | No |
| b | 35 | Yes | No |
| c | 54 | No | Yes |
| d | 55 | No | Yes |
| e | 43 | No | No |
| f | 60 | Yes | No |
| g | 60 | Yes | No |
| h | 55 | No | Yes |
| i | 60 | Yes | No |
| j | 14 | No | No |

Figure S3. Table describing the properties of grain boundaries present in the region in Figure 4.

| Grain Boundary (s) | Average misorientation (deg) | Is a twin boundary? | Strain localization |
|---|---|---|---|
| a | 60 | Yes | No |
| b | 53 | No | Yes |
| c | 60 | Yes | No |
| d | 22 | No | No |
| e | 60 | Yes | No |
| f | 52 | No | Yes |
| g | 57 | No | Yes |

Figure S4. Table describing the properties of grain boundaries present in the region in Figure 5.

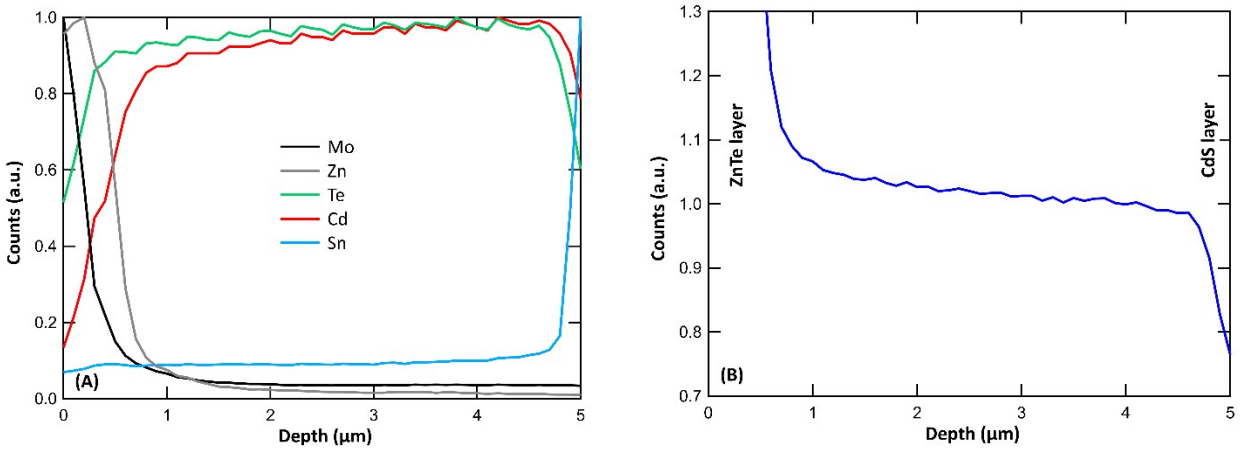


Figure S5. (A) Depth profiles of Mo, Zn, Te, Cd, Sn obtained from fitting of the XRF data that were obtained in a multi-modal approach simultaneously to XRD data. The counts for all elements correspond to the integral of the K-line peaks from fitting all XRF spectra of the 3D data set, were next summarized over the horizontal 2D layers, and normalized to the maximum number of counts for each element individually. The increase of the count rates of Cd and Te with depth is likely caused by increasing thickness (the pillar had a slightly cone-like shape rather than a perfect cylinder). (B): Te/Cd ratio based on the data shown in (A). Beyond the enhanced Te concentration at the ZnTe/CdTe interface and the enhanced Cd concentration at the CdTe/CdS interface, a decrease of the Te concentration in the bulk is observed towards the CdS layer, which is in agreement with the diffusion of S into the bulk from the CdS layer.